Spin and charge excitations in artificial hole- and electron-doped infinite layer cuprate superconductors

G. Dellea,[1] M. Minola,[1,*] A. Galdi,[2,†] D. Di Castro,[3] C. Aruta,[3] N.B. Brookes,[4] C. J. Jia,[5] C. Mazzoli,[1,‡] M. Moretti Sala,[4] B. Moritz,[5] P. Orgiani,[6] D. G. Schlom,[7] A. Tebano,[8] G. Balestrino,[8] L. Braicovich,[9] T. P. Devereaux,[10] L. Maritato,[6] and G. Ghiringhelli[1,§]

[1]*CNR-SPIN and Dipartimento di Fisica, Politecnico di Milano,*
piazza Leonardo Da Vinci 32, Milano, I-20133, Italy;

[2]*CNR-SPIN and Dipartimento di Ingegneria dell'Informazione,*
Ingegneria Elettrica e Matematica Applicata-DIEM,
Università di Salerno, I-84084 Fisciano (SA), Italy;

[3]*CNR-SPIN and Dipartimento di Ingegneria Civile e Ingegneria Informatica,*
Universit di Roma Tor Vergata, Via del Politecnico 1, I-00133 Roma, Italy;

[4]*European Synchrotron Radiation Facility,*
71 Avenue des Martyrs, Grenoble F-38043, France;

[5]*Stanford Institute for Materials and Energy science,*
SLAC National Accelerator Laboratory and Stanford University,
Menlo Park, California 94025, USA

[6]*Dipartimento di Ingegneria Industriale-DIIN,*
Università di Salerno and CNR-SPIN, I-84084 Fisciano (SA), Italy;

[7]*Department of Materials Science and Engineering,*
and Kavli Institute for Nanoscale Science,
Cornell University, Ithaca, New York 14853, USA;

[8]*CNR-SPIN and Dipartimento di Ingegneria Civile e Ingegneria Informatica,*
Università di Roma Tor Vergata, Via del Politecnico 1, I-00133 Roma, Italy;

[9]*CNR-SPIN and Dipartimento di Fisica, Politecnico di Milano,*
piazza Leonardo Da Vinci 32, Milano, I-20133, Italy;

[10]*Stanford Institute for Materials and Energy science,*
SLAC National Accelerator Laboratory and Stanford University,
Menlo Park, California 94025, USA;

(Dated: August 12, 2017)

Abstract

The asymmetry between electron- and hole-doping in high critical-temperature superconducting (HTS) cuprates is key information for the understanding of Cooper pairs formation mechanisms. Despite intensive studies on different cuprates, a comprehensive description of related magnetic and charge excitations is still fragmentary. In the present work, artificial cuprates were used to cover the entire phase diagram within the same HTS family. In particular, Cu L_3-edge resonant inelastic x-ray scattering (RIXS) measurements were performed on artificial n- and p-type infinite layers (IL) epitaxial films. Beside several similarities, RIXS spectra show noticeable differences in the evolution, with doping level, of magnetic and charge intensity and damping. Compatible trends can be found in spectra measured on bulk cuprates, as well as in theoretical calculations of the spin dynamical structure factor $S(\mathbf{q}, \omega)$. The findings give a deeper insight about the evolution of collective excitations across the cuprate phase diagram, and on underlying general features, only connected to the doping type. Moreover they pave the way to the exploration of general properties of HTS physics over a broad range of conditions, by means of artificial compounds not constrained by the thermodynamic limitations governing the chemical stability of bulk materials.

PACS numbers: 74.25.Jb, 74.72.-h, 78.70.Ck

I. INTRODUCTION

Resonant inelastic x-ray scattering (RIXS) has been recently used to study the low energy excitations ($E < 1\ eV$), including spin-flip ones[1], in several cuprate high T_c superconductors (HTS)[2]. This class of experiments is particularly valuable because it probes the set of collective and local excitations that are supposedly involved with the basic mechanisms of high temperature superconductivity. In particular, high resolution RIXS at Cu$-L_3$ edge has been used to measure the magnon dispersion in undoped insulating cuprates[3–6], and damped spin excitations (paramagnons) in hole-doped (h-doped) cuprates. It has thus been shown that paramagnons persist throughout the phase diagram, from superconducting under- and optimally-doped[7–9] to non-superconducting highly-overdoped[10] samples. Paramagnons have also been observed in the prototypical electron-doped (e-doped) cuprate compound $Nd_{2-x}Ce_xCuO_4$ (NCCO)[11,12]. These findings have triggered several works[7,13–15], aiming to show that paramagnons are the driving excitations in Cooper pair formation. However there is no obvious correlation between the critical temperature (T_c) and the paramagnon energy, and this may indicate that also other low energy excitations play a role, such as phonons (via electron-phonon coupling) and charge modes[11,12,16]. It is then worth studying the low energy excitations in cuprate compounds with different structure, in order to identify their correlations with high temperature superconductivity.

A striking characteristic of the class of cuprate HTS is the marked asymmetry between the phase diagram of h and e-doped compounds: some important physical proprieties, such as pseudogap, charge order and maximum T_c, dramatically change from the h-doped to the e-doped side[17,18]. Experiments show that also the paramagnon excitations have a different doping evolution upon hole and electron doping: for h-doped compounds the dispersion is almost unaffected by doping, while for e-doped ones the dispersion is doping dependent, with hardening of the paramagnon mode up to 50%[11,12]. This asymmetry can be correctly captured by a relatively simple model including three-site exchange[19], even though there is no perfect agreement with the experimental dispersion data[11,12].

It is worth noting that HTS of e- and h-doped type typically descend from parent compounds with different crystal structure[20], and this can indeed affect the low energy excitation spectrum[21]. Conversely a direct quantitative comparison with theory[19] would greatly benefit from a measurement made on cuprates with the same crystal symmetry, changing doping only from holes to electrons. To this aim ambipolar cuprates, that can be doped with holes and electrons, do not offer a sufficiently wide doping range, not even displaying superconductivity on the e-doped side[22].

In order to provide a suitable system for the study of the doping asymmetry of magnetic excitations in cuprates, we employed advanced thin film growth techniques to obtain h- and e-doped cuprates with infinite layer (IL) structure. IL cuprates are particularly interesting because of their crystallographic structure: the simplest among layered cuprates. On the other hand, the IL compounds are metastable and single crystal can be stabilized only in thin film form[23–28].

E-doping of the IL compound $Sr_{1-x}La_xCuO_2$ (SLCO) is obtained via Sr substitution with La in the $SrCuO_2$ parent compound, attaining maximum T_c of 42K for $x = 0.1$[29,31]. SLCO is an e-doped cuprate with different structure than NCCO and other T' e-doped compounds[17,18]. It is then also worth to determine whether the low energy excitations studied by RIXS have the same behavior in the two families of e-doped cuprates.

In order to get h-doping of ILs, a different approach is necessary: it takes advantage of recent progresses in epitaxial growth, and is based on a proper engineering of heterostructures and superlattices (SLs)[32,34–37]. These synthetic HTS, not constrained to thermodynamic limitations connected with bulk crystal growth, are particularly interesting in the search of increasing T_c.

In the present work, $(CaCuO_2)_n/(SrTiO_3)_m$ ($(CCO)_n/(STO)_m$) SLs were used to achieve h-doped IL superconductors, while SLCO thin films grown on $GdScO_3$ are the investigated e-doped samples. These samples offer the unique possibility of probing the evolution of magnetic excitations as a function of doping in the same cuprate system going from e-doped to h-doped superconducting phase.

II. EXPERIMENTAL

A. Sample preparation

Electron doped SLCO thin films ($x = 0, 0.08, 0.10, 0.13$) were grown on $GdScO_3$ substrates by layer-by-layer molecular-beam epitaxy aided and calibrated by reflection high-energy electron diffraction in a reactive atmosphere of O_3. Superconductivity is achieved via an in situ vacuum annealing step, which results in oxygen loss from the films. The infinite layer structure was confirmed by x-ray diffraction analysis.[28,38] The superconducting transition temperatures of the analyzed films depends on the La content ($x = 0.08, 0.10$ and 0.13) and corresponds to: $T_c = 27.8, 28$ and 19.5 K respectively.

Pulsed laser deposition (PLD) was used to synthesize $(\mathrm{CCO})_n/(\mathrm{STO})_m$ SLs made by 20 repetitions of n unit cells of CCO and m unit cells of STO, on $NdGaO_3$ (110) substrates. Superconducting SLs were grown at 600°C in a mixture of oxygen and 12% ozone atmosphere at a pressure of about 1 mbar. X-ray diffraction and HRTEM characterization indicates the formation of high structural quality superlattices with sharp interfaces[32,34]. In these samples h-doping was verified by Hall effect and x-ray absorption measurements at Cu L_3 edge and an estimate of the doping level was given[32]: the measured carrier density, rescaled to the thickness of the $CaCuO_2$ layers, results in doping of 0.14 holes per Cu ion for $n = 3$ SLs. It was demonstrated that the hole doping is obtained via control of the oxygen content at the CCO/STO interface, with oxygen-rich interfaces introducing holes in the cuprate layer[34,39]. The superconducting SLs analyzed are $(\mathrm{CCO})_n/(\mathrm{STO})_2$ with: $n = 13$, $T_c = 12$ K (thick CCO layer); $n = 7$, $T_c = 16$ K (intermediate CCO layer); $n = 3$, $T_c = 25$ K (thin CCO layer). The non-superconducting $(\mathrm{CCO})_3/(\mathrm{STO})_2$ SL is obtained by growing the sample in oxygen, so that the oxygen content at the interface is reduced. Resistivity measurements and x-ray absorption spectra confirm that the sample can be considered undoped[32].

B. Cu L_3-edge RIXS

The Cu L_3-edge RIXS experiments were performed at the ID08 beamline of the European Synchrotron Radiation Facility (ESRF), using the AXES spectrometer. The combined energy resolution of the beam line monochromator and the spectrometer was 250 and 265 meV for $(\mathrm{CCO})_n/(\mathrm{STO})_m$ SLs and SLCO film measurements, respectively. The temperature was kept at 20 K for all measurements. We tuned the incident photon energy to the maximum of the Cu$-L_3$ adsorption edge (i.e. resonant to the Cu^{2+} ions in the CuO_2 planes) and used linearly polarized x-rays parallel to the scattering plane (π-polarization). The scattering geometry of the experiment is shown in Figure1 a): the photon momentum $\mathbf{K}_{\mathrm{in}}$ is determined by the energy of the Cu $2p - 3d$ resonant transition, the maximum transferred

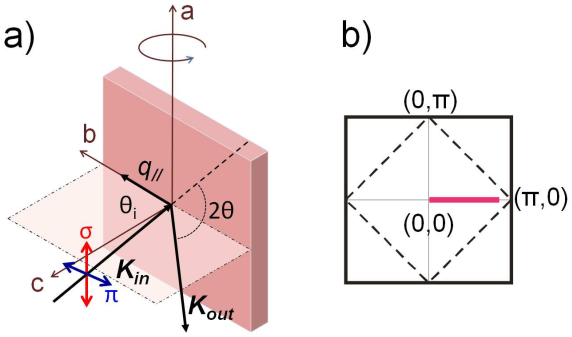

FIG. 1. (color online) (a) Experimental setup layout and (b) reciprocal space region spanned inside the first Brilluoin Zone.

momentum $\mathbf{q}$ is that given by the fixed scattering angle $2\theta = 130°$. Although this is fixed, the projection of $\mathbf{q}$ onto the ab-plane ($\mathbf{q}_{||}$) can be changed by rotating the sample around the axis perpendicular to the scattering plane, allowing to measure dispersing features. In this way, the region of the 2D reciprocal space indicated by magenta solid line in Figure1(b) can be accessed. The maximum $q_{||} = |\mathbf{q}_{||}|$ is 0.7 Å^{-1}, corresponding to 0.435 reciprocal lattice units (r.l.u.). The possibility to neglect the momentum variations along the c axis is related to the strongly 2D nature of the system, which also determines the electronic properties of the material. The chosen experimental configuration (π incident photon polarization, and $\mathbf{q}_{||} = (h > 0, 0)$) enhances the spin flip signal as compared to other excitation channels.[40]

C. DQMC theoretical calculations on $S(q, \omega)$

The RIXS cross section was numerically evaluated directly from the Kramers-Heisenberg formula using small-cluster exact-diagonalization (ED) of an effective single-band Hubbard Hamiltonian (including both nearest t and next nearest neighbor hopping t' and on-site Coulomb repulsion U) at various electron concentrations N and as a function of momentum transfer, as explained in detail in references 19 and 41. The spin dynamical structure factor, $S(\mathbf{q}, \omega)$, was determined by a numerically exact dynamic quantum Monte Carlo (DMQC) method with maximum entropy analytic continuation on large lattices.

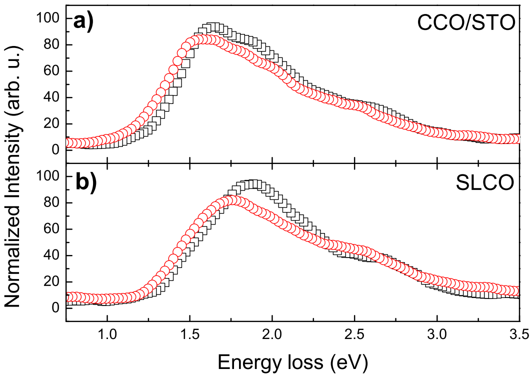

FIG. 2. (color online) *dd* excitation spectra of (a) $(CCO)_3/(STO)_2$ SLs: undoped (black squares) and optimally doped (red circles);(b)undoped SCO (black squares) and optimally doped (red circles). The spectra have been measured with $\mathbf{q}_{\|} = (0.37, 0)$ and π polarization. The spectra have been normalized to the spectral weight in the energy range $[1, 3.5]$ eV equal to 100.

III. RESULTS

In Figure 2 we report the RIXS spectra of undoped and optimally doped $(CCO)_3/(STO)_2$ SLs (panel (a)) and SLCO (panel (b)) in the energy range associated to the *dd* excitations. The *dd* excitations of the undoped SL sample reproduce the spectrum observed in CCO single films reported in ref. 40. The features of the SLCO spectra appear broader, most probably because of the tendency of SLCO to accept interstitial oxygen defects[24–28]. Despite the different type of doping the spectra show very similar behavior upon introduction of extra carriers: the electronic features broaden and shift to lower energy in both h- and e-doped cases.

Figure 3 presents a general overview of the momentum and doping dependence for the two types of materials. Since a direct measurement of the absolute scattering intensity is not possible in soft RIXS experiments, all spectra in Figure 3 were normalized to the spectral weight in the energy range associated to *dd* excitations (i.e. between 1 and 3.5 eV)[39,40] set equal to 100, in order to allow direct comparisons. In panel (b) the two antiferromagnetic (AFM) parent compounds are directly compared; a distinct feature emerges from the elastic peak at zone center (Γ point) for both AFM samples, it disperses toward higher energies with increasing momentum and reaches its maximum ($\sim$ 300 meV) towards the zone boundary (ZB) at (π, 0). Notably, this spectrum feature is almost perfectly superimposed for both

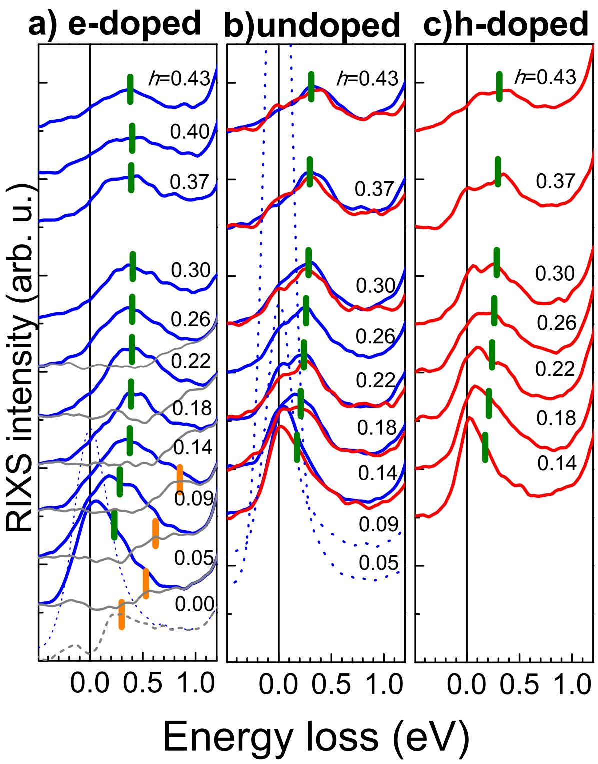

FIG. 3. (color online)(a-c) Cu$-L_3$ edge RIXS raw spectra waterfall plots of momentum dependence as a function of doping type, measured with π incident polarization along the $(0,0)$ - $(\pi,0)$ direction. The in-plane transferred momentum is defined as $\mathbf{q}_{\parallel} = (h,0)$ with h expressed in r.l.u. SLCO spectra are denoted with blue lines, while $(\mathrm{CCO})_n/(\mathrm{STO})_m$ spectra are defined with red lines. Green ticks indicate the (para)magnon position as estimated by fitting procedure. Orange thick lines give the fast dispersing charge peak. (a) optimally e-doped doped sample: SLCO with $x = 0.1$ and $T_c = 28$ K. Thin grey lines represent the residual RIXS intensity after subtraction of the elastic and paramagnon peak, revealing the presence of the fast dispersing mode.(b) Insulating AFM parent compounds: SCO (blue solid lines) and not superconducting $(\mathrm{CCO})_3/(\mathrm{STO})_2$ (red solid lines). (c) h-doped best superconducting sample: $(\mathrm{CCO})_3/(\mathrm{STO})_2$ with $T_c = 25$ K.

undoped $\mathrm{SrCuO_2}$ (SCO) (blue line) and $(\mathrm{CCO})_3/(\mathrm{STO})_2$ (red line), validating the assumption of considering equivalent SCO and CCO in the AFM state. Panels (a) and (c) show the corresponding spectra for n- and p-type doped samples: SLCO ($x = 0.10$) and superconducting $(\mathrm{CCO})_3/(\mathrm{STO})_2$ respectively. Raw data clearly display some differences in the low energy scale for different type of doping. Furthermore the spectra decomposition (described in next paragraph, see Figure 4) reveals an additional dispersing feature in e-doped SLCO,

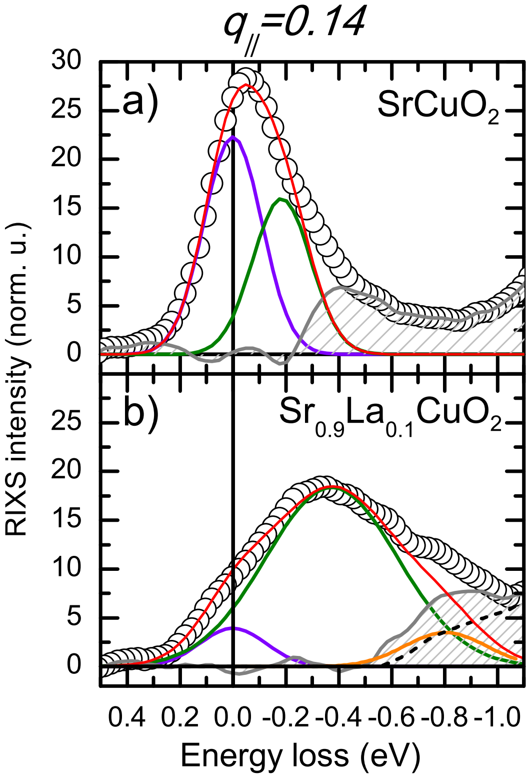

FIG. 4. (color online)Examples of spectra decomposition in the low energy region, at $q_{\|} = 0.14$ r.l.u. and π incident polarization, for (a) undoped $SrCuO_2$ and (b) optimally e-doped SLCO. The data are plotted with circles, while lines are used to plot the Gaussian components: elastic peak (purple), magnon (green), charge mode (orange), tail of *dd* excitations and $q_{\|}$-independent continuum background (black dashed); the thin red line represents the sum of all the components. The shadowed region in (a) is the residual intensity attributed to multi-magnon or charge continuum and to the tail of *dd* excitations. The same approach is used for undoped and h-doped SLs.

not observed in h-doped SLs. In bulk crystals of NCCO a similar peak was recognized as a charge signal and associated either to particle-hole excitations within the upper Hubbard band[11] or to a different quantum phase[12].

The low energy part of the spectra was decomposed so to identify the (para)magnon and other relevant low energy excitations; an example of the decomposition is shown in Figure 4 (a) for the SCO case and in Figure 4 (b) for the $x = 10\%$ SLCO sample. The spectra of undoped samples were fitted following a procedure already employed on insulating bulk cuprates[3] and SLs[42]: two resolution-limited Gaussians were used for the elastic peak (purple solid line), and the magnon (green solid line); remaining spectral weight close to 500 meV energy loss was associated to multiple magnons, and an additional phonon contribution at 100 meV was considered for SL[42]. For superconducting samples, the decomposition process is less evident. We chose to fit the spectra with a resolution limited Gaussian for the elastic peak (purple solid line) and non-resolution-limited Gaussians for the magnetic inelastic peak (green solid line) as shown in Figure 4 (b).

The free fitting parameters are the area of the elastic Gaussian component A_{el}, the energy position E_i, area A_i and width w_i of the inelastic component. We associate to E_i an error bar equal to three times the standard deviation associated by the fitting procedure, after verifying that this is sufficient to include the error due to parameter correlations. The fitted elastic and paramagnon contributions have been subtracted from the raw data. The residual background is independent from $q_{||}$ for the h-doped SLs, while for the e-doped samples it shows a $q_{||}$ dependence for $q_{||} < 0.22$ r.l.u., as shown by the residual RIXS intensity plotted by thin grey lines in Figure 3(a). The comparison with NCCO RIXS spectra reported in literature[11,12] provides support for the introduction of an additional non-resolution-limited inelastic component in our fitting procedure, represented by the orange line in Figure 4 (b).

The results of the decomposition procedure are displayed in Figure 5. In Figure 5(a) we compare the spectra of the undoped, h-doped and e-doped samples at fixed $\mathbf{q}_{||}$, highlighting the width of the inelastic Gaussian component (horizontal bar), and the intensity associated to the energy range $[0.8, 1.2]$ eV (vertical bar). The broadening of the magnetic excitation peak, stronger for the e-doping case, is an intrinsic phenomenon, suggesting that we are dealing with dynamical magnetic fluctuations[7]. The increase of the spectral weight around $0.8 - 1.2$ eV is attributed to the filling of continuum states associated to doping carriers[7]. At equivalent doping levels, the charge contribution given by e-doping is stronger compared to h-doping.

In Figure 5(b) the inelastic peak positions are reported as a function of $q_{||}$, so that the energy dispersion of the magnetic and charge excitations can be determined. The dispersion of the magnetic component (i.e. the single non-elastic component) in the undoped parent compounds presents the typical evolution of spin waves in an antiferromagnetic square lattice, consistent with what already found in previous RIXS experiments on undoped bulk cuprates[3–5] and SLs[6,42]. The dispersing peak in h-doped sample closely mimics the magnon

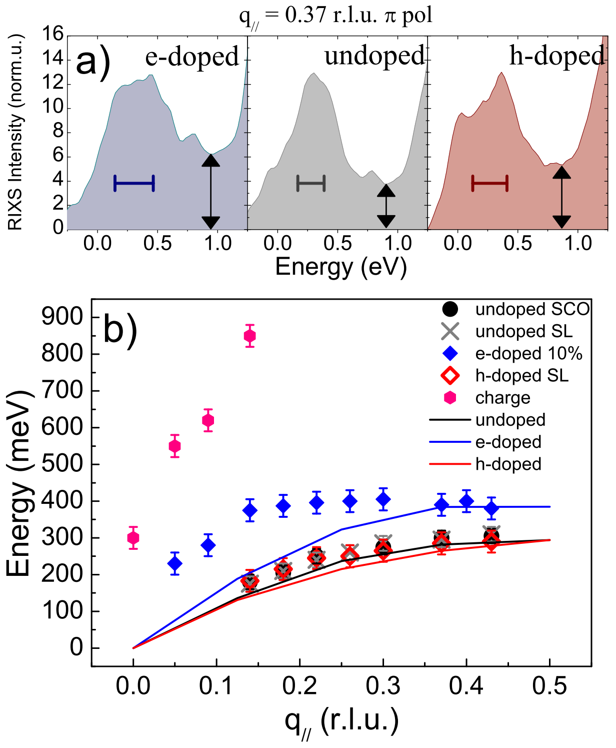

FIG. 5. (color online)(a) Cu$-L_3$ edge RIXS raw spectra of non superconducting SCO(black), best superconducting $(\mathrm{CCO})_3/(\mathrm{STO})_2$ (red) and optimally doped SLCO (blue), at $q_\parallel = 0.37$ r.l.u. and $T = 20$ K, measured with π incident polarization. Intensities are normalized to have the same height on the (para)magnon peak. Horizontal solid line represents the FWHM of the (non-)resolution limited Gaussian used to decompose the data. Vertical arrows indicates the intensity in the energy range $[0.8, 1.5]$ eV, where continuum excitations appear upon doping. Plotting undoped SL instead of SCO would lead to the same conclusions. (b) (Para)magnon dispersion (black circle: undoped SLCO, black cross: undoped SL, red open diamonds: $(\mathrm{CCO})_3/(\mathrm{STO})_2$, blue filled diamonds: SLCO $x = 0.1$) and fast dispersing charge mode (pink hexagons) as deduced from RIXS spectra compared to $S(\mathbf{q}, \omega)$ theoretical calculations in a single band Hubbard model (black line: no doping, red line: hole doping, blue line: electron doping) with nearest hopping parameter $t = 500$ meV. Experimental error bars correspond to three times the standard deviation associated to the fitting parameter.

peak observed in AFM parent compounds whereas the e-doped paramagnon presents a steeper dispersion: faster at lower $q_\parallel$ (≤ 0.18 r.l.u.) and almost flat for higher $q_\parallel$. A significant hardening in energy (20% at ZB), compared to undoped and h-doped case, is also evident in SLCO.

The additional inelastic peak in the e-doped sample, associated to charge excitations, is resolved for $q_{\parallel} < 0.18$ r.l.u., whereas for higher $q_{\parallel}$, it becomes impossible to distinguish it from the *dd* excitation peaks, so that we can identify only one inelastic non-resolution-limited component. The charge mode irradiates from the Γ point and moves rapidly towards higher energy with increasing $q_{\parallel}$. As mentioned above, similar excitations have been observed in RIXS measurements on the prototypical e-doped cuprate NCCO[11,12], with the same steep dispersion we find in SLCO, as shown in Figure 5 (b).

IV. DISCUSSION

The data reported in Figure 3(b) show that the undoped IL SCO and $(CCO)_3/(STO)_2$, present the same dispersion of magnon excitations, with maximum energy of ~ 300 meV moving towards the zone boundary along $\Gamma - X$, despite their different composition and nanostructure. A further confirmation is given by the very similar *dd* excitations shown in Figure 2. This allows us to consider the two systems as equivalent and to directly compare for the first time the evolution of magnetic excitations as a function of doping from electrons to holes in the very same infinite-layer cuprate system. H-doped spectra in Figure 3(c) were fitted ascribing the inelastic spectral weight to a single non-resolution-limited magnetic component. A dispersing paramagnon is clearly visible (see Figure 5(b)), similar to what found in bulk h-doped samples[7–10]: the magnetic peak gets damped and broadened, but preserves its spectral weight and momentum dependence similar to those of the AFM parent compound. Our RIXS results thus demonstrate that magnetic excitations in superconducting SLs preserve the behavior observed in bulk crystals, even when hole doping is induced via oxygen-rich interfaces in artificial heterostructures.

The peak decomposition is less straightforward for superconducting e-doped sample in Figure 3(a). To take into account the experimental evidence, according to what was done in Ref.[11,12], at lower $q_{\parallel}$ (< 0.18 r.l.u.) the non-elastic spectral weight was decomposed into two non-resolution-limited components: a magnetic peak and a charge feature. The dispersion of paramagnon and charge excitations reported in Figure 5(b), qualitatively reproduces the findings in bulk NCCO confirming the generality of the results: the observed strong asymmetry between the magnetic dispersions of h- and e-doped samples and the fast dispersing charge mode are indeed general features connected to electron doping and not related to the particular type of sample investigated or method of growth.

In Figure 5(b) we also report the comparison of the experimental dispersion with theoretical calculation of the dynamic spin structure factor $S(\mathbf{q}, \omega)$, shown to be a good description of the RIXS signal, even without outgoing polarization analysis,[19] thanks to our choice of scattering geometry enhancing spin-flip excitations. The numerical data are in good agreement, both qualitatively and quantitatively, with the undoped and h-doped experimental points, while the agreement is less good for e-doping. The lack of agreement is particularly evident for lower $q_{\|}$ values, where the dispersion is steeper, while theoretical curves reproduces the paramagnon energy data close to the ZB. One possible explanation for this discrepancy is the observed strong itinerant character of the electron doped copper oxides, evidenced by the enhanced spectral weight around $0.8 - 1.5$ eV.[11] It is well known that the RIXS cross section[1,19] of cuprates for incident π polarization and large positive $q_{\|}$ values is dominated by single spin-flip excitations, whereas at lower $q_{\|}$ charge excitations give a more significant contribution, mixing with spin-flip excitations in the same energy range. More in detail, the charge contribution can account for up to $\sim$20% of the signal even at high $q_{\|}$ values[43] thus complicating an accurate determination of the paramagnon energy. This contamination from the charge channel is obviously not taken into account in $S(\mathbf{q}, \omega)$ calculations and might be at the origin of the discrepancies between numerical and experimental data. Future measurements including polarization analysis will clarify whether this is indeed the case or if the current model is not adequate enough to describe the magnetic response of e-doped compounds.

In Figure 6, spectra at fixed $\mathbf{q}_{\|} = (0.37, 0)$ r.l.u. are compared with calculated $S(\mathbf{q}, \omega)$ for different electron filling N, where $N = 1$ represents the zero-doping condition (half filling). The chosen momentum transfer is close enough to the ZB to assure a good agreement between experimental data and theoretical predictions. SLCO filling is estimated according to La dopants stoichiometry (x) as $N = 1 + x$, while for $(\mathrm{CCO})_n/(\mathrm{STO})_m$ N is related to $\mathrm{CaCuO_2}$ layer thickness (n): the thicker the $\mathrm{CaCuO_2}$ layer, the lower the average doping per $\mathrm{CuO_2}$ plane. The best situation is obtained for $n = 3$ (0.14 holes/Cu, from Hall measurements[32] and recent optical conductivity measurements[33]), corresponding to $N = 0.86$. STEM/EELS measurements on single CCO/STO interfaces[34] show that the holes are substantially present only in the first 1-2 unit cells from the interface. So, we can still associate a filling level to the n=3 SL. On the other hand, in larger period SLs the inner CuO_2 planes are not doped anymore, in analogy to what found for layered HTS compounds[47,48]. Consequently it is not possible to associate a filling level for the $n = 7$ ($T_c = 16\ K$) and $n = 13$ ($T_c = 12\ K$) SLs, whose spectra are rather a superposition of doped and undoped $CaCuO_2$; we report them for comparison in Figure 6(a), with T_c values as labels. The magnetic peak energy is unchanged within our experimental resolution going from $N = 1$ to $N = 0.86$ and this trend is confirmed by the behavior of the large period SLs. A good qualitative agreement between theory and experiments is again evident: h-doped samples present a magnetic peak almost independent on doping level, while the magnetic peak of e-doped samples strongly evolves for increasing doping and shifts to higher energies.

V. CONCLUSIONS

We have investigated the evolution of low energy excitations of hole and electron doped IL cuprates. In particular, to the best of our knowledge, we studied for the first time the doping dependence of (para)magnon excitations, going from h-doped to e-doped cuprate compounds without changing the crystal structure. In analogy with the observations in NCCO,[11,12] magnetic excitation harden significantly with e-doping, in stark contrast with hole-doping behavior. This result is counterintuitive: the AFM correlations are presumably short-ranged for any doping. To reconcile this apparent discrepancy, the e-doping hardening has been interpreted as signature of the strongly itinerant character of e-doped materials as compared to the more localized spin dynamics found in h-doped cuprates.[11] This asymmetry between doping types is also well caught within the single-band Hubbard model, as proved by the good agreement between $S(\mathbf{q}, \omega)$ calculations and experimental results.[19] Our data also confirm the existence of a fast dispersive charge mode present in all e-doped materials but absent in h-doped samples. Our assignment of this mode to charge excitations is supported by the polarization dependence of Cu$-L_3$ RIXS data and also Cu$-K$ RIXS measurements on e-doped crystals[11,45]. The origin of this mode, emanating from zone center and rapidly decaying in intensity, is still unclear. Some authors interpreted it as intraband particle-hole excitation,[11] whereas others proposed that it is the signature of a quantum phase distinct from superconductivity[12] or a plasmon excitation:[45] in any case this mode is a general feature of all e-doped cuprates. In conclusion, our results prove the feasibility of studying magnetic and charge excitations of cuprate superconductors by using a new generation of artificial epitaxial materials, not constrained by thermodynamic limitations and whose physical properties (such as doping level, oxygen content, T_c) can be controlled by properly tuning the growing conditions. This will open new and unexplored directions of investigations on superconducting cuprates. Moreover the data are available for direct comparison with future theoretical models aimed at understanding the strong asymmetry in collective excitations between the two sides of the cuprate phase diagram, which we proved to be a general property not due to the differences in composition and structure of the materials investigated. Finally, it should be stressed that, due to limited amount of material present in SLs and thin films, soft RIXS is the only viable technique for investigating charge and magnetic excitations in these artificial superconducting cuprates. Further improvements in the comprehension of our findings, especially for the fast dispersing charge mode and the paramagnon dispersion at low $q_{\|}$, will likely come also from future experiments using the newest high-resolution RIXS spectrometers, allowing also full analysis of the scattered polarization[49,50].

ACKNOWLEDGMENTS

This work made use of the Cornell Center for Materials Research Shared Facilities which are supported through the NSF MRSEC program (DMR-1120296). The RIXS experiment was made at the beam line ID08 of the ESRF using the AXES spectrometer, property of the CNR and managed jointly by the Politecnico di Milano and the ESRF. GD was supported by the H2020 COST action TO-BE (#MP1308). GD, MM and GG were supported by the PIK-POLARIX project of the Italian Ministry of Research (MIUR).

VI. REFERENCES

---

[*] Present address: Max-Planck-Institut für Festkörperforschung, Heisenbergstrasse 1, D-70569 Stuttgart, Germany.

[†] agaldi@unisa.it

[‡] Present address: National Synchrotron Light Source II, Brookhaven National Laboratory, Upton, New York 11973, USA.

[§] giacomo.ghiringhelli@polimi.it

[1] L.J.P. Ament, G. Ghiringhelli, M.M. Sala, L. Braicovich, and J. van den Brink, Phys. Rev. Lett. **103**, 117003 (2009).

[2] M.P.M. Dean, J. Magn. Magn. Mater. **376**, 3 (2015).

[3] L. Braicovich, L.J.P. Ament, V. Bisogni, F. Forte, C. Aruta, G. Balestrino, N.B. Brookes, G.M. De Luca, P.G. Medaglia, F. Miletto Granozio, M. Radovic, M. Salluzzo, J. van den Brink, and G. Ghiringhelli, Phys. Rev. Lett. **102**, 167401 (2009).

[4] M. Guarise, B. Dalla Piazza, M. Moretti Sala, G. Ghiringhelli, L. Braicovich, H. Berger, J.N. Hancock, D. van der Marel, T. Schmitt, V.N. Strocov, L.J.P. Ament, J. van den Brink, P.-H. Lin, P. Xu, H.M. Rønnow, and M. Grioni, Phys. Rev. Lett. **105**, 157006 (2010).

[5] L. Braicovich, M. Moretti Sala, L.J.P. Ament, V. Bisogni, M. Minola, G. Balestrino, D. Di Castro, G.M. De Luca, M. Salluzzo, G. Ghiringhelli, and J. van den Brink, Phys. Rev. B 81, 174533 (2010).

[6] M.P.M. Dean, R.S. Springell, C. Monney, K.J. Zhou, J. Pereiro, I. Božović, B. Dalla Piazza, H.M. Rnnow, E. Morenzoni, J. van den Brink, T. Schmitt, and J.P. Hill, Nat. Mater. 11, 850 (2012).

[7] M. Le Tacon, G. Ghiringhelli, J. Chaloupka, M.M. Sala, V. Hinkov, M.W. Haverkort, M. Minola, M. Bakr, K.J. Zhou, S. Blanco-Canosa, C. Monney, Y.T. Song, G.L. Sun, C.T. Lin, G.M. De Luca, M. Salluzzo, G. Khaliullin, T. Schmitt, L. Braicovich, and B. Keimer, Nat. Phys. 7, 11 (2011).

[8] M.P.M. Dean, G. Dellea, R.S. Springell, F. Yakhou-Harris, K. Kummer, N.B. Brookes, X. Liu, Y.-J. Sun, J. Strle, T. Schmitt, L. Braicovich, G. Ghiringhelli, I. Božović, and J.P. Hill, Nat. Mater. 12, 1019 (2013).

[9] M.P.M. Dean, A. J. A. James, R.S. Springell, X. Liu, C. Monney, K.J. Zhou, R.M. Konik, J.S. Wen, Z.J. Xu, G.D. Gu, V.N. Strocov, T. Schmitt, and J.P. Hill, Phys. Rev. Lett. 110, 147001 (2013).

[10] M. Le Tacon, M. Minola, D.C. Peets, M. Moretti Sala, S. Blanco-Canosa, V. Hinkov, R. Liang, D.A. Bonn, W.N. Hardy, C.T. Lin, T. Schmitt, L. Braicovich, G. Ghiringhelli, and B. Keimer, Phys. Rev. B 88, 020501 (2013).

[11] K. Ishii, M. Fujita, T. Sasaki, M. Minola, G. Dellea, C. Mazzoli, K. Kummer, G. Ghiringhelli, L. Braicovich, T. Tohyama, K. Tsutsumi, K. Sato, R. Kajimoto, K. Ikeuchi, K. Yamada, M. Yoshida, M. Kurooka, and J. Mizuki, Nat. Commun. 5, 3714 (2014).

[12] W.S. Lee, J.J. Lee, E. A. Nowadnick, S. Gerber, W. Tabis, S.W. Huang, V.N. Strocov, E.M. Motoyama, G. Yu, B. Moritz, H.Y. Huang, R.P. Wang, Y.B. Huang, W.B. Wu, C.T. Chen, D.J. Huang, M. Greven, T. Schmitt, Z.X. Shen, and T.P. Devereaux, Nat. Phys. 10, 883 (2014).

[13] M.T. Béal-Monod, C. Bourbonnais, and V.J. Emery, Phys. Rev. B 34, 7716 (1986).

[14] D.J. Scalapino, Rev. Mod. Phys. 84, 1383 (2012).

[15] Miyake, Schmitt-Rink, and Varma, Phys. Rev. B. 34, 6554 (1986).

[16] Y.Y. Peng, M. Hashimoto, M.M. Sala, A. Amorese, N.B. Brookes, G. Dellea, W.-S. Lee, M. Minola, T. Schmitt, Y. Yoshida, K.-J. Zhou, H. Eisaki, T.P. Devereaux, Z.-X. Shen, L. Braicovich, and G. Ghiringhelli, Phys. Rev. B 92, 064517 (2015).

[17] N.P. Armitage, P. Fournier, and R.L. Greene, Rev. Mod. Phys. 82, 2421 (2010).

[18] P. Fournier, Phys. C Supercond. Its Appl. 514, 314 (2015).

[19] C.J. Jia, E. a Nowadnick, K. Wohlfeld, Y.F. Kung, C.-C. Chen, S. Johnston, T. Tohyama, B. Moritz, and T.P. Devereaux, Nat. Commun. 5, 3314 (2014).

[20] M.A. Kastner, R.J. Birgeneau, G. Shirane, and Y. Endoh, Rev. Mod. Phys. 70, 897 (1998).

[21] M.P.M. Dean, A.J.A. James, A.C. Walters, V. Bisogni, I. Jarrige, M. Hücker, E. Giannini, M. Fujita, J. Pelliciari, Y.B. Huang, R.M. Konik, T. Schmitt, and J.P. Hill, Phys. Rev. B 90, 220506 (2014).

[22] K. Segawa, M. Kofu, S.-H. Lee, I. Tsukada, H. Hiraka, M. Fujita, S. Chang, K. Yamada, and Y. Ando, Nat. Phys. 6, 579 (2010).

[23] E. Koller, L. Mieville, L. Fàbrega, J.M. Triscone, and O. Fischer, Phys. C 235-240, 707 (1994).

[24] J. Tomaschko, V. Leca, T. Selistrovski, S. Diebold, J. Jochum, R. Kleiner, and D. Koelle, Phys. Rev. B 85, 024519 (2012).

[25] R. Feenstra, X. Li, M. Kanai, T. Kawai, S. Kawai, J.D. Budai, E.C. Jones, Y.R. Sun, J.R. Thompson, S.J. Pennycook, and D.K. Christen, Phys. C Supercond. Its Appl. 224, 300 (1994).

[26] Z.Z. Li, V. Jovanovic, H. Raffy, and S. Megtert, Phys. C Supercond. Its Appl. 469, 73 (2009).

[27] A. Gupta, B.W. Hussey, T.M. Shaw, A.M. Guloy, M.Y. Chern, R.F. Saraf, and B.A. Scott, J. Solid State Chem. 112, 113 (1994).

[28] L. Maritato, A. Galdi, P. Orgiani, J.W. Harter, J. Schubert, K.M. Shen, and D.G. Schlom, J. Appl. Phys. 113, 053911 (2013).

[29] M.G. Smith, A. Manthiram, J. Zhou, J.B. Goodenough, and J.T. Markert, Nature 351, 549 (1991).

[30] G. Er, Y. Miyamoto, F. Kanamaru, and S. Kikkawa, Phys. C 181, 206 (1991).

[31] Jorgensen, Radaelli, Hinks, Wagner, Kikkawa, Er, and Kanamaru, Phys. Rev. B. Condens. Matter 47, 14654 (1993).

[32] D. Di Castro, M. Salvato, A. Tebano, D. Innocenti, C. Aruta, W. Prellier, O.I. Lebedev, I. Ottaviani, N.B. Brookes, M. Minola, M. Moretti Sala, C. Mazzoli, P.G. Medaglia, G. Ghiringhelli, L. Braicovich, M. Cirillo, and G. Balestrino, Phys. Rev. B 86, 134524 (2012).

[33] A. Perucchi, P. Di Pietro, S. Lupi, R. Sopracase, A. Tebano, G. Giovannetti, F. Petocchi, M. Capone, D. Di Castro, arXiv:1708.00390.

[34] D. Di Castro, C. Cantoni, F. Ridolfi, C. Aruta, A. Tebano, N. Yang, and G. Balestrino, Phys. Rev. Lett. 115, 147001 (2015).

[35] D. Di Castro, C. Aruta, A. Tebano, D. Innocenti, M. Minola, M. Moretti Sala, W. Prellier, O. Lebedev, and G. Balestrino, Supercond. Sci. Technol. 27, 44016 (2014).

[36] F. Arciprete, G. Balestrino, S. Martellucci, P.G. Medaglia, A. Paoletti, and G. Petrocelli, Appl. Phys. Lett. 71, 959 (1997).

[37] D.P. Norton, D.H. Lowndes, and J.D. Budai, Appl. Surf. Sci. 98, 672 (2008).

[38] J.W. Harter, L. Maritato, D.E. Shai, E.J. Monkman, Y. Nie, D.G. Schlom, and K.M. Shen, Phys. Rev. B 92, 035149 (2015).

[39] C. Aruta, C. Schlueter, T.-L. Lee, D. Di Castro, D. Innocenti, A. Tebano, J. Zegenhagen, and G. Balestrino, Phys. Rev. B 87, 155145 (2013).

[40] M. Moretti Sala, V. Bisogni, C. Aruta, G. Balestrino, H. Berger, N.B. Brookes, G.M. De Luca, D. Di Castro, M. Grioni, M. Guarise, P.G. Medaglia, F. Miletto Granozio, M. Minola, P. Perna, M. Radovic, M. Salluzzo, T. Schmitt, K.J. Zhou, L. Braicovich, and G. Ghiringhelli, New J. Phys. 13, 043026 (2011).

[41] C. Jia, K. Wohlfeld, Y. Wang, B. Moritz, and T.P. Devereaux, Phys. Rev. X 6, 021020 (2016).

[42] M. Minola, D. Di Castro, L. Braicovich, N.B. Brookes, D. Innocenti, M. Moretti Sala, A. Tebano, G. Balestrino, and G. Ghiringhelli, Phys. Rev. B 85, 235138 (2012).

[43] M. Minola, G. Dellea, H. Gretarsson, Y.Y. Peng, Y. Lu, J. Porras, T. Loew, F. Yakhou, N.B. Brookes, Y.B. Huang, J. Pelliciari, T. Schmitt, G. Ghiringhelli, B. Keimer, L. Braicovich, M. Le Tacon, Phys. Rev. Lett. 114, 217003 (2015).

[44] L. Braicovich, M. Moretti Sala, L.J.P. Ament, V. Bisogni, M. Minola, G. Balestrino, D. Di Castro, G.M. De Luca, M. Salluzzo, G. Ghiringhelli, and J. van den Brink, Phys. Rev. B 81, 174533 (2010).

[45] K. Ishii, K. Tsutsui, Y. Endoh, T. Tohyama, S. Maekawa, M. Hoesch, K. Kuzushita, M. Tsubota, T. Inami, J. Mizuki, Y. Murakami, and K. Yamada, Phys. Rev. Lett. 94, 207003 (2005).

[46] R.S. Markiewicz, M.Z. Hasan, and A. Bansil, Phys. Rev. B 77, 094518 (2008).

[47] B. A. Scott, E. Y. Suard, C. C. Tsuei, D. B. Mitzi, T. R. McGuire, B.-H. Chen, and D. Walker, Physica C 230, 239 (1994).

[48] A. Iyo, Y. Tanaka, Y. Kodama, H. Kito, K. Tokiwa, and T. Watanabe, Physica C 445, 17 (2006).

[49] G. Ghiringhelli and L. Braicovich, J. Electron Spectros. Relat. Phenomena 188, 26 (2013).

[50] L. Braicovich, M. Minola, G. Dellea, M. Le Tacon, M. Moretti Sala, C. Morawe, J.-C. Peffen, R. Supruangnet, F. Yakhou, G. Ghiringhelli, and N.B. Brookes, Rev. Sci. Instrum. 85, 115104 (2014).

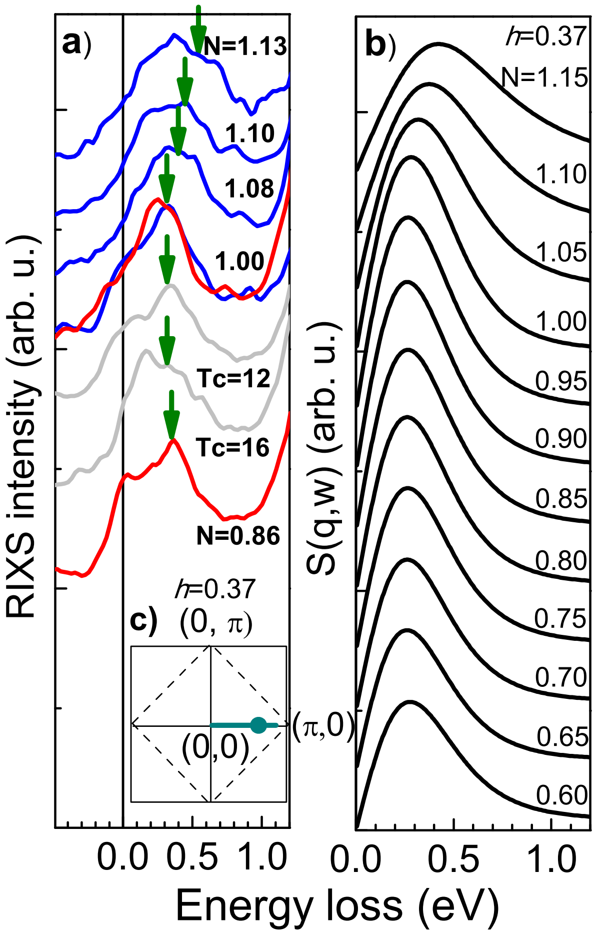

FIG. 6. (color online)Filling dependence at fixed transferred momentum: comparison between raw RIXS spectra and dynamic spin structure factor $S(\mathbf{q},\omega)$ in single band Hubbard model. (a) Raw RIXS spectra of SLCO are denoted with blue lines, SLs $(\mathrm{CCO})_3/(\mathrm{STO})_m$ are defined with red lines, while non-homogeonously doped $n = 7, 13$ SLs are reported with grey lines. Green arrows are guide for the eyes and indicate the (para)magnon position as estimated by fitting procedure. (b) Quantum Monte Carlo (DQMC) simulations of the dynamic spin structure factor $S(\mathbf{q},\omega)$ at $(3/4\pi, 0)$ in the single band Hubbard model as a function of N. (c) Schematic picture of the first Brillouin zone with dashed lines denoting the AFM ZB. Green solid line highlights the entire RIXS available region of the reciprocal space, while green dot indicates the $\mathbf{q}_{\|}$ selected in panels (a) and (b).